Journal of Catalysis 257 (2008) 142–151

Contents lists available at ScienceDirect

Journal of Catalysis

www.elsevier.com/locate/jcat

Impact of Cr, Mn and Zr addition on Fe Fischer–Tropsch synthesis catalysis: Investigation at the active site level using SSITKA

Nattaporn Lohitharn, James G. Goodwin Jr. *

Department of Chemical and Bimolecular Engineering, Clemson University, Clemson, SC 29634, USA

ARTICLE INFO

Article history:
Received 14 February 2008
Revised 16 April 2008
Accepted 19 April 2008
Available online 23 May 2008

Keywords:
Fischer–Tropsch synthesis (FTS)
CO hydrogenation
Methanation
Steady-state isotopic transient kinetic analysis (SSITKA)
Cr promotion
Mn promotion
Zr promotion
Water–gas shift (WGS)
Fe-based FTS catalysts

ABSTRACT

Recently, we reported that Cr, Mn, or Zr promotion of a precipitated Cu-promoted Fe Fischer–Tropsch synthesis (FTS) catalyst significantly improves its catalytic activity. In this study, we used steady-state isotopic transient kinetic analysis (SSITKA) of methanation to investigate the activity of these catalysts at the site level, providing insight into how this promotion enhances catalyst activity. We found that the activity of the base Fe catalyst was enhanced by promotion with Cr, Mn, and Zr in varying degrees, depending on the type and concentration of metal added. The addition of these third metals promoted the dispersion of Fe but did not significantly affect either the BET surface area or reducibility. The activities of the reaction sites (estimated by $1/\tau_{CH_4} = \mathrm{TOF}_{\mathrm{ITK}}$) were found to be similar regardless of the type of third metal added, suggesting that the active sites for Fe catalysts with or without third-metal promotion were essentially identical. The higher catalyst activities observed for the Cr-, Mn-, and Zr-promoted Fe catalysts were found to be due primarily to an increased number of active surface intermediates leading to hydrocarbon products.

1. Introduction

Due to the limited supply and unpredictable price of crude oil, increasing attention has focused on other energy sources, including coal, natural gas, and biomass. The U.S. has 25% of the world's coal reserves, which is sufficient to supply most of the U.S. liquid transportation fuel needs for more than 100 years with the use of Fischer–Tropsch synthesis (FTS) [1]. FTS is an excellent method for upgrading low-value coal and biomass to high-value, environmentally friendly liquid fuels with no sulfur contamination [2,3]. A catalyst with high water–gas shift (WGS) activity is needed to use the low-H_2/CO ratio syngas derived from coal or biomass.

Fe-based catalysts have great potential to convert low-H_2 source syngas to fuels via FTS due to their high WGS activity and low cost compared with Co-based catalysts. Development of Fe catalysts with high FTS activity, low methane selectivity, and long-term stability is of great importance. It has been shown that the addition of some transition metals to Fe-based FTS catalysts improves these catalysts' activity and selectivity. Increases in chain growth probability and catalyst activity from the addition of Cr to a precipitated Fe catalyst have been reported [4]. Very stable activity and high selectivity to light olefin formation have been observed for Mn-promoted Fe catalysts [5–8]. A positive affect of other transition metals, such as Mo, Ta, V, and Zr, on the catalyst activity for both CO hydrogenation and WGS activity also has been reported [8].

Previous studies have explored how the addition of Cr [4], Mn [5,6,9], or Zr [10] affects the activity of Fe FTS catalysts. Recent work by us in a comparative study of third-metal promotion also has demonstrated that the addition of Cr, Mn, and Zr significantly enhances the activity of a typical precipitated Cu- and SiO_2-promoted Fe catalyst [8]. Little is known about how Cr, Mn, or Zr promotion affects the kinetic nature of the Fe catalyst active sites, however. Most investigations to date have used *ex situ* characterization techniques to evaluate catalysts' physicochemical properties under conditions far different than reaction conditions. Speculation on the nature of the active sites during reaction based on the findings of such studies has the potential for significant error. Steady-state isotopic transient kinetic analysis (SSITKA) can provide *in situ* surface kinetic information about a reaction on a catalyst under actual reaction conditions. In the present study, we used SSITKA to determine the concentration of active surface intermediates leading to products and the intrinsic site activities of the catalysts, with the aim of gaining insight into how Cr, Mn, and Zr influence the activity of Fe catalysts. We also explored the effect of varying Cr, Mn, and Zr concentrations on the catalyst activity for both CO hydrogenation and the WGS reaction.

* Corresponding author. Fax: +1 864 656 0784.
E-mail address: jgoodwi@clemson.edu (J.G. Goodwin).

0021-9517/$ – see front matter
doi:10.1016/j.jcat.2008.04.015

2. Experimental

2.1. Catalyst preparation

Catalysts were prepared using a pH precipitation technique [11] according to the general formulations of 100Fe/5Cu/17Si (base catalyst) and $(100-x)$Fe/xMe/5Cu/17Si (on an atomic basis), where Me is Cr, Mn, or Zr and x is $\leqslant 20$. The details of the catalyst preparation method used in this study can be found elsewhere [8]. In brief, a mixed aqueous solution containing $Fe(NO_3)_3{\cdot}9H_2O$, $CuN_2O_6{\cdot}3H_2O$, and $Si(OC_2H_5)_4$ without a third metal species for 100Fe/5Cu/17Si and with a third metal species [$Cr(NO_3)_3$, $Mn(NO_3)_2$, or $ZrO(NO_3)_2$] for $(100-x)$Fe/xMe/5Cu/17Si was precipitated with NH_4OH at 83 °C to achieve a pH of 8–9. The precipitate was aged at room temperature for 17 h (overnight) to allow it to cool completely, and then thoroughly washed with deionized water. The washed precipitate was dried at 110 °C for 18–24 h and calcined in air at 300 °C for 5 h. The catalysts were sieved to <90 μm. The catalyst nomenclatures used are 100Fe, 97Fe3Cr, 95Fe5Cr, 93Fe7Cr, 90Fe10Cr, 95Fe5Mn, 93Fe7Mn, 90Fe10Mn, 80Fe20Mn, 97Fe3Zr, 95Fe5Zr, 90Fe10Zr, and 86Fe14Zr for the benchmark and Cr-promoted Fe catalysts at 3, 5, 7, and 10 at% of Cr, Mn-promoted Fe catalysts at 5, 7, 10, and 20 at% of Mn, and Zr-promoted Fe catalysts at 3, 5, 10, and 14 at% of Zr, respectively. Metal at% is based on 100Fe for the benchmark catalyst. Total (Fe + the third metal) at% is 100. General catalyst nomenclatures for Cr-, Mn-, Zr-, and third metal-promoted Fe catalysts are FeCr, FeMn, FeZr, and FeMe, respectively.

2.2. Catalyst characterization

2.2.1. BET surface area

N_2 physisorption at 77 K was used to determine the BET surface areas using a Micromeritics ASAP 2020 automated system. A 0.3-g sample was degassed under a vacuum of 10^{-3} mm Hg at 100 °C for 1 h, after which the temperature was raised to 300 °C (at a rate of 10 °C/min) and held there for 2 h before N_2 adsorption.

2.2.2. Catalyst composition

The carbon content of catalysts after reaction and the elemental composition of the fresh calcined catalysts were analyzed using a combustion method and inductively coupled plasma optical emission spectrometry (ICP-OES), respectively, by Galbraith Laboratories Inc. (Knoxville, TN). Passivation was performed for spent catalysts before they were removed from the reactor, to prevent rapid oxidation on exposure to air, by introducing a flow of 40 cc/min of 2% O_2 in He to the catalyst bed at ca. 35 °C. A ca. 5–7 °C increase in catalyst temperature was observed during passivation. Passivation was considered complete once the temperature of the catalyst bed dropped back to the original temperature.

2.2.3. X-ray diffraction

Powder XRD was conducted to determine the crystallinity of fresh calcined catalysts using a Scintag 2000 X-ray diffractometer with monochromatized CuK_α radiation (40 kV, 40 mA) and a Ge detector. A step scan mode was used at a scan rate of 0.02° (2θ) per second from 10–80°.

2.2.4. Scanning electron microscopy and energy-dispersive X-ray spectroscopy

The morphologies of the catalyst samples and the elemental distributions and concentrations of the exterior catalyst particle surfaces were studied by SEM and EDX, respectively, using a Hitachi FESEM-S4800 under the scanning electron (SE) mode. The accelerating voltage was 20 kV with a working distance of 14 mm.

2.2.5. Temperature-programmed reduction

H_2 TPR (ambient to 800 °C at 2 °C/min) was performed using an Altamira AMI-1 system to measure the reducibility of Fe. A 0.1-g sample of a freshly calcined catalyst was reduced in a flow of 30 cc/min of 5% H_2/Ar. A variation of TPR was also performed in which the temperature was increased to 280 °C (2 °C/min) and held there for 12 h, to mimic the reduction conditions before the reaction. Then the temperature was increased to 800 °C at 2 °C/min, and the additional H_2 consumed was measured. The H_2 consumption was determined by a thermal conductivity detector (TCD) calibrated based on 100% reducibility of Ag_2O powder using the same heating rate. A cold trap was placed before the TCD to trap H_2O produced during the TPR process.

2.2.6. CO chemisorption

The concentration of surface metal atoms was determined using CO chemisorption in a Micromeritics ASAP 2010 automated system. A 0.1-g sample of a freshly calcined catalyst was first evacuated to 10^{-6} mm Hg at 100 °C for 30 min and then reduced under flowing H_2 by ramping at 2 °C/min to 280 °C and holding there for 12 h. The catalyst was then evacuated at 280 °C for 60 min to desorb H_2. CO chemisorption was carried out at 35 °C. An average CO:Fe_s stoichiometry of 1:2 was assumed [12].

2.3. Reaction kinetic measurements

The reaction was carried out in a differential quartz microreactor (8 mm i.d.). The reaction conversion was kept below 10% to minimize temperature and concentration gradients. A 35- to 100-mg catalyst sample was reduced *in situ* at 280 °C (after ramping at 2 °C/min) under 30 C/min of H_2 (National Specialty Gases, zero grade) for 12 h. Then 30 cc/min of He (National Specialty Gases, UHP) was used to purge the catalyst for 15 min before the reaction at 280 °C and a constant pressure of 1.8 atm. The total flow rate of the reaction mixture was kept constant at 60 cc/min (STP) containing 5 cc/min of 95% CO + 5% Ar (National Specialty Gases) and 10 cc/min of H_2 in He balance, to obtain a H_2:CO ratio of 2:1. The reaction effluent line and the sampling valves were maintained at 200 °C with heating tape, to avoid condensation of higher hydrocarbon products. The effluent samples were analyzed using a Varian 3700 gas chromatograph equipped with an AT-Q 30 m × 0.53 mm Heliflex capillary column with a flame ionization detector (FID) for hydrocarbon detection and a Carbosphere 80/100 6′ × 1/8″ × 0.085″ SS packed column with a TCD for CO and CO_2 detection.

2.4. Steady-state isotopic transient kinetic analysis

SSITKA was performed by switching ^{12}CO (containing 5% Ar) and ^{13}CO (Isotec, 99%) without disturbing the other reaction conditions, using a Valco 2-position valve with an electric actuator. The total flow rate and reaction pressure of these two feed streams were identical during the switch. A small trace of Ar was present in the unlabelled ^{12}CO stream, to measure the gas-phase holdup for the reaction system. The reaction was carried out at the same conditions as described above but with a H_2:CO ratio of 20:1, to obtain CH_4 as the primary product. Thus, the reaction mixture comprised 1.5 cc/min of 95% CO + 5% Ar, 30 cc/min of H_2, and 28.5 cc/min of He. The effluent gas was analyzed online with a Varian 3700 gas chromatograph and a Balzers–Pfeiffer Prisma 200 amu quadrupole mass spectrometer (Pfeiffer Vacuum) via a 1/16-inch capillary tube with differential pumping. The gas inlet line to the mass spectrometer was designed to be as short as possible, to minimize gas-phase holdup in the system, and was heated to 150 °C to avoid the deposition of heavy hydrocarbon products. The mass spectrometer was equipped with a high-speed data-acquisition system interfaced

Table 1
BET surface area and elemental composition of the various Fe-based catalysts

Catalyst[a]	BET SA[b] (m^2/g)	Me/Fe atomic ratio[c]	
		Bulk[d]	Particle surface[e]
100Fe	329	0	0
97Fe3Cr	346	0.030	0.036
95Fe5Cr	354	0.053	0.054
93Fe7Cr	358	0.074	0.076
90Fe10Cr	331	0.098	0.117
95Fe5Mn	354	0.050	0.066
93Fe7Mn	361	0.074	0.072
90Fe10Mn	365	0.107	0.099
80Fe20Mn	381	0.218	0.241
97Fe3Zr	335	0.034	0.040
95Fe5Zr	337	0.063	0.069
90Fe10Zr	339	0.133	0.140
86Fe14Zr	328	0.176	0.170

[a] All catalysts also contained 5Cu and 17Si.
[b] Max error = ±5%.
[c] Me = Cr, Mn, or Zr.
[d] ICP-OES results. Max error = ±5%.
[e] EDX results. Max error = ±8%.

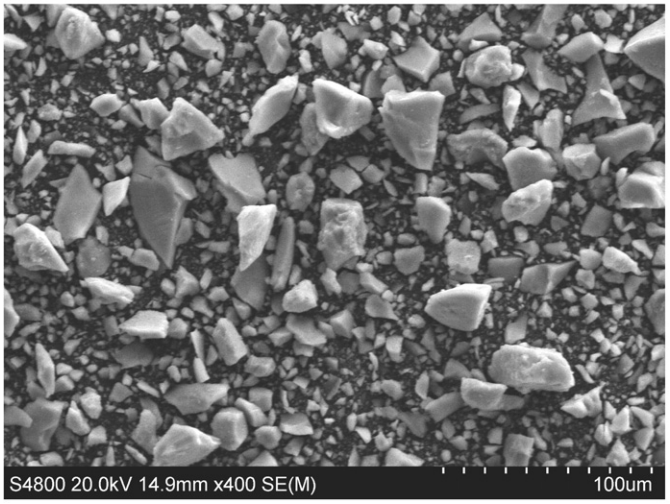

Fig. 1. SEM micrographs of calcined 90Fe10Zr.

to a personal computer using Balzers Quadstar 422 v 6.0 software. Surface kinetic parameters, the average surface residence time of CH_4 and of CO (τ_{CH_4} and τ_{CO}), and the active surface concentrations of CH_x (leading to CH_4) and of CO (N_{CH_4} and N_{CO}), were determined from the isotopic transients using SSITKA data analysis software [13,14].

3. Results and discussion

3.1. Catalyst characterization

3.1.1. BET surface area

Table 1 gives the BET surface areas of the catalysts. Slightly higher BET surface areas (0–14%) were found for the Fe catalysts with Cr, Mn, or Zr promotion compared with the benchmark 100Fe catalyst. Taking into account experimental error, the BET surface areas of the Zr-promoted Fe catalysts and 100Fe were essentially identical, and those of the Cr- and Mn-promoted catalysts were greater than that of 100Fe, with that of FeMn the largest.

3.1.2. XRD

XRD of all of the fresh calcined and spent Fe catalysts revealed no discernible diffraction peaks for any oxide or metal phase of Fe, Cr, Mn, Zr, or Cu (results not shown). This suggests that all of the catalysts were XRD amorphous due to small crystallites of the various metal oxides.

3.1.3. SEM and EDX

Figs. 1 and 2 show catalyst granule morphologies and elemental distributions on the surface of the freshly calcined 90Fe10Zr particles detected by SEM and EDX, respectively. The particles were irregularly shaped with facets and were similar for all catalysts (not shown). Although Cr, Mn, and Zr were added at relatively high concentrations, they did not interfere with the distribution of the other elements. All elements contained in the catalyst were well dispersed evenly over all of the Fe catalyst particles, with no obvious segregation. Based on the finding that all Fe catalysts were XRD amorphous, the catalyst particles detected by SEM must have been composed of thousands of very small Fe oxide crystallites bound together but prevented from sintering by SiO_2 [15], which also acted as a binding agent [16]. Thus, higher BET surface areas were obtained compared with that of a typical precipitated Fe catalyst with no SiO_2 present [17]. In addition, comparing the ratio of Me/Fe present in the bulk and on the surface of the catalyst particles as determined using ICP-OES and EDX, respectively (Table 1), shows a uniform distribution of the third metal (Me) and Fe (i.e., the ratio of Me/Fe on the particle surface was similar to that of the bulk composition).

3.1.4. Temperature-programmed reduction

Fig. 3 shows TPR profiles of Fe catalysts with the addition of Cr, Mn, and Zr. No significant difference in the reduction behavior was detected in the Fe catalysts with and without third-metal promotion. All of the catalysts exhibited similar reduction peaks as those seen in a pure Fe_2O_3 powder but at lower reduction temperatures, due to the presence of Cu (which is well known to facilitate the reduction of Fe [2,18]). Two distinct reduction peaks were observed at around 215–280 °C and 605 °C, attributed to the reduction of $Fe_2O_3 \rightarrow Fe_3O_4$ and $Fe_3O_4 \rightarrow Fe$, respectively [19,20]. Obtaining an absolute value of %Fe reducibility for a complicated catalyst system containing multiple metals (as well as possible multiple oxide phases of Fe) is not straightforward. Because it is possible that some Fe_2O_3 could have been reduced to Fe_3O_4 and then rapidly to Fe in the presence of Cu, the calculation of %Fe reducibility was based on an assumption that Fe_2O_3 was reduced to Fe^0.

In previous work [8], we obtained only a reduction equivalent to the first TPR reduction peak of Fe under standard reduction conditions (i.e., ramping to 280 °C at 2 °C/min and holding for 12 h) before the reaction. Therefore, the reducibility results reported in Table 2 include only those determined from the first reduction peak. We found that %reducibility of Fe was in the range of 32%–41% and was not affected by the type of metal added or its concentration. But reduction peak temperatures did vary slightly among the catalysts with different types of added metal and different concentrations; for example, the reduction peak temperature for the FeCr catalysts shifted to higher values, and a small shoulder peak at ~210 °C became more noticeable with increasing %Cr loading (Fig. 3a). Comparing the small shoulder peak at 210 °C of 90Fe10Cr with a reduction peak temperature of a 100Cr/5Cu/17Si sample (no Fe present; see Fig. 3a) at 215 °C shows that this small shoulder peak may have resulted from the partial reduction of Cr_2O_3 [21].

A shift of the first reduction peak to higher temperatures also was observed for the Mn-promoted Fe catalysts (Fig. 3b). This apparently suggests that reduction of Fe was more difficult in the presence of Mn, possibly due to the ability of MnO to stabilize Fe^{2+} [22–24]. The existence of mixed-oxide phases between Fe_3O_4 and Mn_3O_4 has been reported for a FeMn catalyst (without Cu or Si present) and has been suggested to inhibit the migration of Fe cations to the surface of catalyst during reduction, inhibiting the

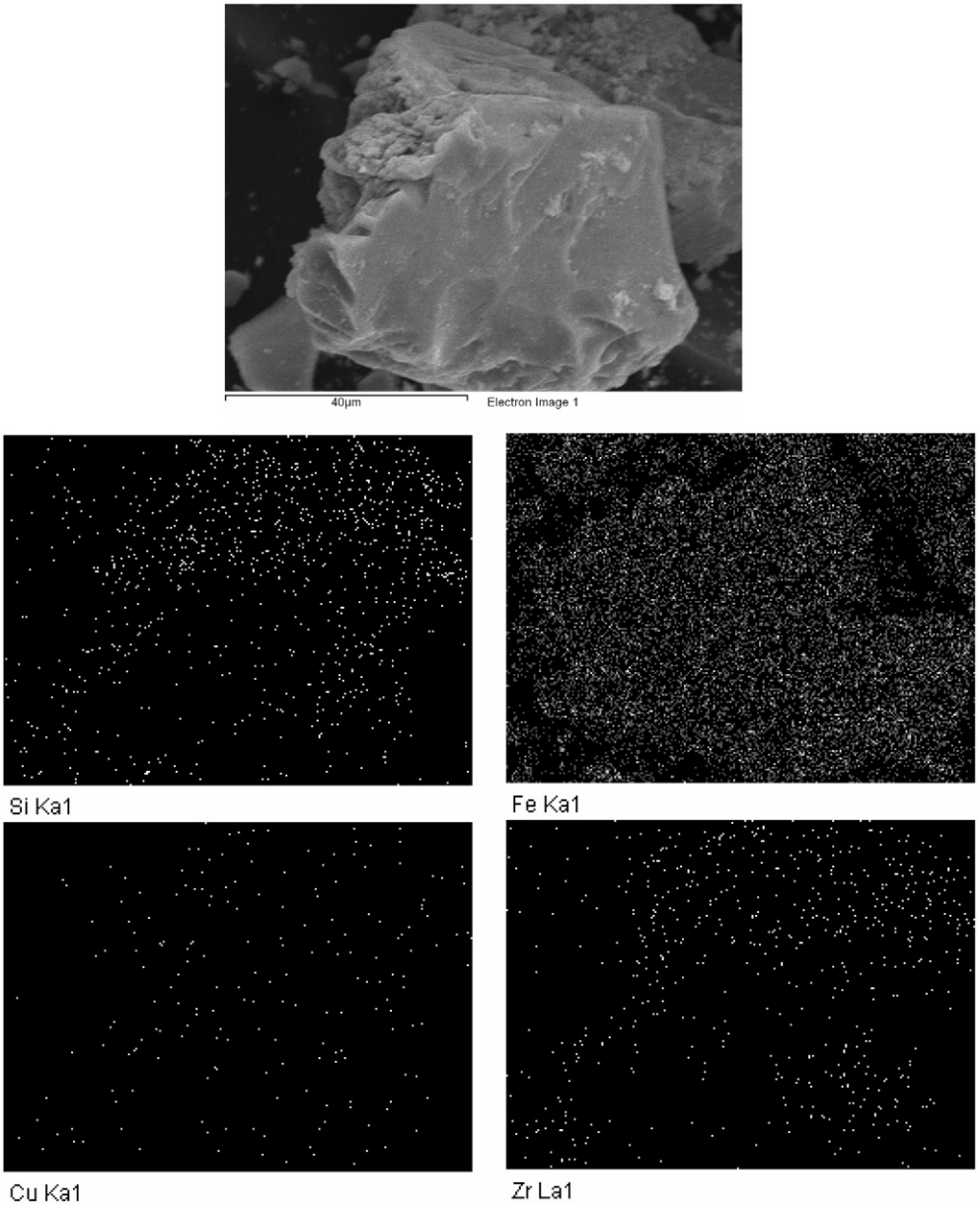

Fig. 2. EDX mapping of a calcined 90Fe10Zr particle.

reduction of Fe [23]. On the other hand, the reduction of Fe was not influenced by the addition of Zr (Fig. 3c). Essentially, the same %Fe reducibilities and reduction peak temperatures were observed for all Zr-promoted Fe catalysts.

3.1.5. CO chemisorption

Table 2 reports the affects of adding Cr, Mn, and Zr on the total CO chemisorption and %Fe dispersion. The amounts of CO chemisorbed were 174–232 µmol/g for FeCr, 140–156 µmol/g for FeMn, and 150–220 µmol/g for FeZr. Because both Fe and the third-metal surface atoms can potentially chemisorb CO, a contribution from chemisorption of CO on Cr, Mn, or Zr was possible. To determine the magnitude of this contribution, we performed CO chemisorption on reduced 100Cr/5Cu/17Si, 100Mn/5Cu/17Si, and 100Zr/5Cu/17Si (no Fe present) using the same procedure as for the 100Fe and FeMe samples. Table 2 reports the total amounts of CO chemisorbed, both uncorrected and corrected, for the FeMe catalysts. These quantities, corrected for the specific amount of Cr, Mn, or Zr, were used to estimate the amount of CO chemisorption on the Fe present in the FeMe catalysts.

Fe catalysts with Cr, Mn, or Zr promotion exhibited greater CO chemisorption and %Fe dispersion than the benchmark 100Fe catalyst regardless of the third-metal loading. The %Fe dispersion was 2.6% for 100Fe, compared with 3.4%–5.8% for the Me-promoted Fe catalysts. These results clearly indicate greater Fe dispersion in the presence of Cr, Mn, or Zr. However, the degree of enhanced Fe dispersion varied, depending on the type and concentration of metal added. The optimum content of added Cr for total CO chemisorption and Fe dispersion was ca. 5 at%. Some surface Fe atoms may have been covered by added Cr at high concentration, leading to a loss of some of the Fe active chemisorption sites and decreased CO chemisorption. A drop in BET surface area also occurred when Cr was added >7 at% (Table 1). In contrast, the amount of surface-exposed Fe appeared to increase with increasing %Zr loading, whereas it was independent of %Mn loading, demonstrating relatively the same Fe dispersion for all of the Mn-promoted Fe catalysts.

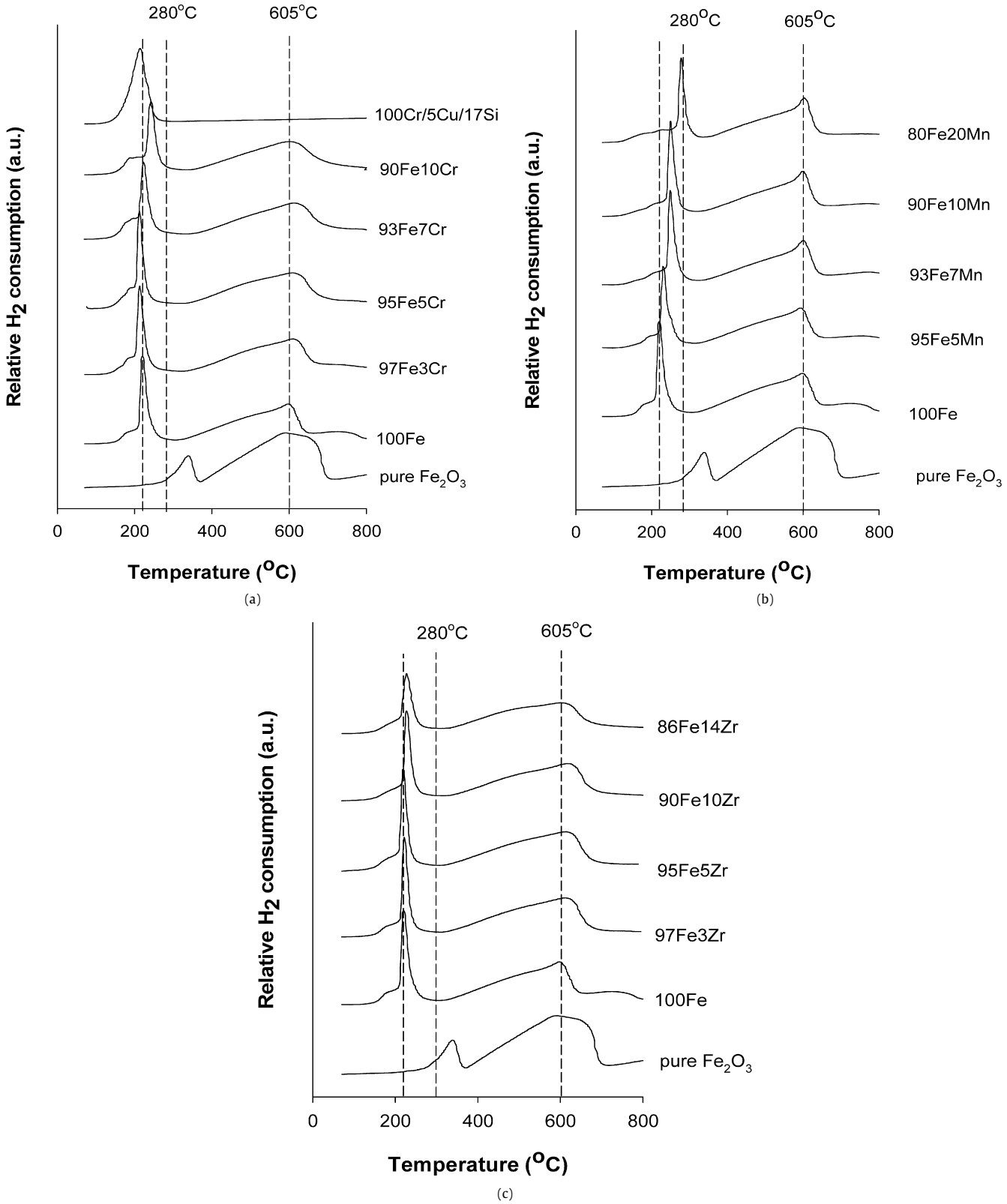

Fig. 3. TPR profiles of calcined (a) Cr-, (b) Mn-, and (c) Zr-promoted Fe catalysts at various %loadings of the 3rd metal.

3.2. Catalyst Activity

3.2.1. Fischer–Tropsch synthesis

We investigated the activities for FTS of Fe-based catalysts with varying concentrations of added Cr, Mn, or Zr at 280 °C, 1.8 atm, and a H_2/CO ratio of 2:1. Previous work [8] demonstrated that the reaction under these conditions and on these catalysts is free from heat or mass-transfer limitations. Figs. 4–6 show the activities for CO hydrogenation and the WGS reaction of the Fe catalysts with Cr, Mn and Zr promotion, respectively. The activities of all of these Fe catalysts exhibited similar induction periods for both reactions, regardless of the type or concentration of metal added. This induc-

Table 2
Results from TPR and CO-chemisorption for the Fe-based catalysts

Catalyst[a]	H_2 TPR (1st peak)		CO-chemisorption		
	Peak temperature[b] (°C)	%Fe reducibility[b]	Total CO chemisorbed[c] (μmol/g)		%Fe dispersion[f]
			Uncorrected[d]	Corrected[e]	
100Fe	220	35	120	–	2.6
97Fe3Cr	213	35	199	187	3.9
95Fe5Cr	212	39	252	232	5.3
93Fe7Cr	222	41	225	197	4.7
90Fe10Cr	242	39	197	174	3.9
95Fe5Mn	241	33	160	155	3.5
93Fe7Mn	249	34	164	156	3.6
90Fe10Mn	251	36	164	154	3.6
80Fe20Mn	278	32	158	140	3.6
97Fe3Zr	222	34	156	150	3.4
95Fe5Zr	217	37	180	169	3.9
90Fe10Zr	229	36	212	191	4.8
86Fe14Zr	227	35	246	220	5.8

[a] All catalysts also contained 5Cu and 17Si.
[b] Max error = ±2%. %Fe reduced in 1st TPR peak. Equivalent to %Fe reduced during standard reduction.
[c] Determined by extrapolating the total chemisorption isotherm to zero pressure.
[d] Total amount of CO chemisorbed without the correction of that on Cr, Mn, or Zr. Max error ±3%.
[e] The contribution of CO chemisorption on Cr, Mn or Zr has been subtracted. Max error ±5%.
[f] Based on total CO chemisorbed (corrected), $CO/Fe_s = 0.5$, %dispersion = 2 × corrected total CO chemisorbed/total number of Fe atoms. Max error ±8%.

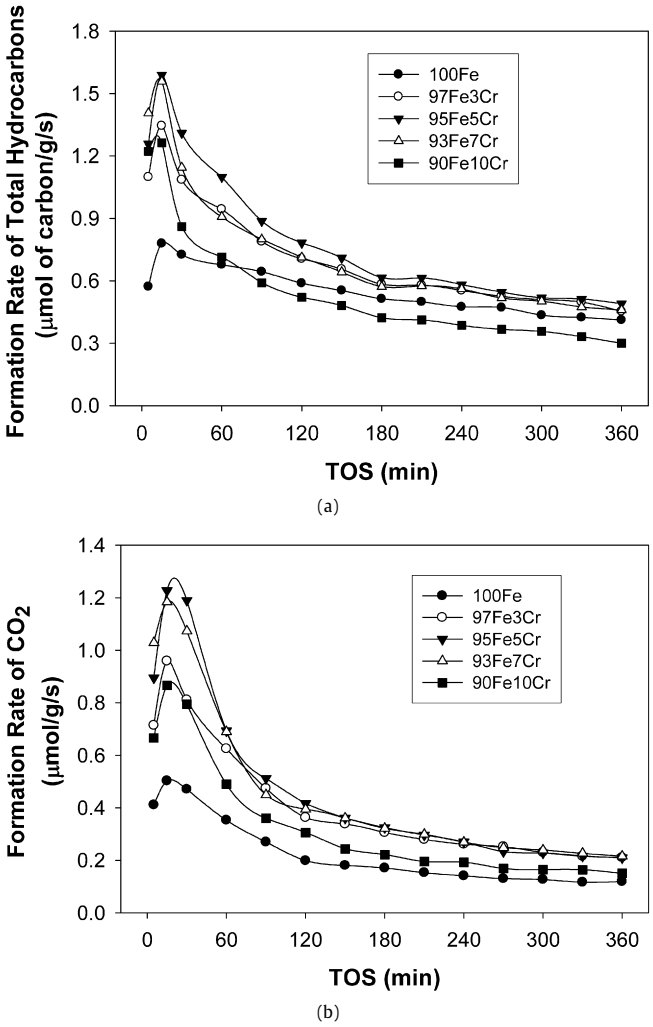

Fig. 4. Formation rates of (a) total hydrocarbons (C_1–C_8) and (b) CO_2 for the Cr-promoted Fe catalysts.

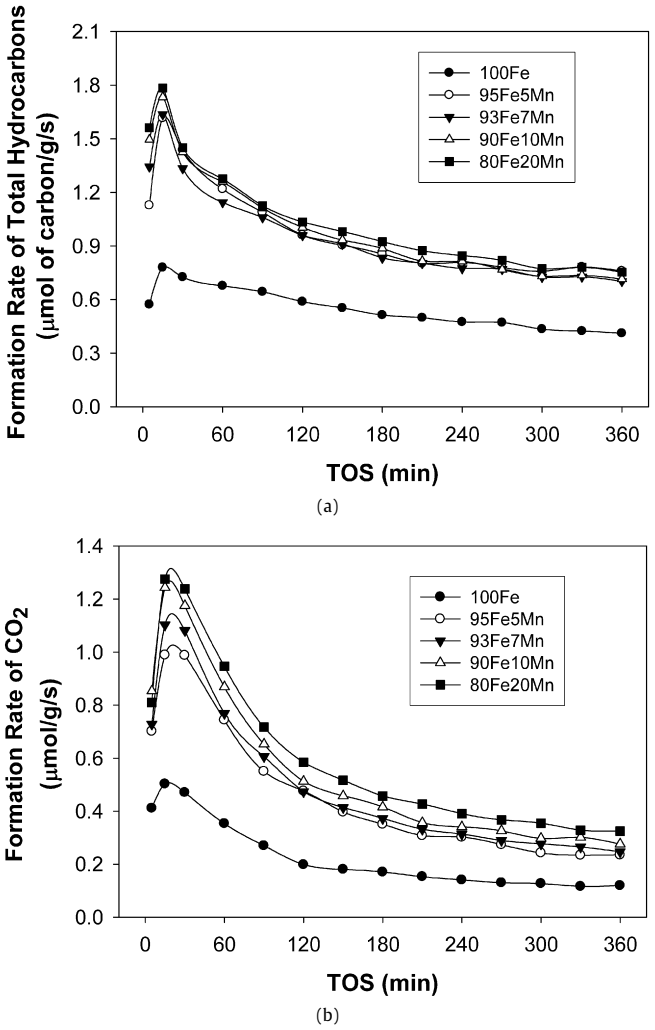

Fig. 5. Formation rates of (a) total hydrocarbons (C_1–C_8) and (b) CO_2 for the Mn-promoted Fe catalysts.

tion period, which has been linked to the time required for the conversion of α-Fe to Fe carbides [25], took approximately 15 min TOS under these reaction conditions.

Figs. 4a and 4b clearly shows that adding Cr at low concentrations (3–7 at%) had a positive affect on catalyst activity, but higher loadings resulted in less activity. Cr at 5 at% was found to be the optimum concentration. The activity of FeCr appears to be directly related to the amount of CO chemisorbed (Table 2). The formation rates of hydrocarbon products and CO_2, on the other hand, increased with increasing Mn content to 20 at% (Fig. 5). The activities of the FeMn catalysts were at least twofold greater than those observed for the benchmark 100Fe catalyst. The initial activities of the Fe catalyst for both CO hydrogenation and the WGS reaction were significantly affected by the concentration of added Zr (Fig. 6). The formation of hydrocarbons and CO_2 during the induction period increased considerably with increasing Zr content. 90Fe10Zr and 86Fe14Zr exhibited such high initial activity that there appeared to be almost no induction period; however, the optimum %loading of Zr was at 10 at% (i.e., 86Fe14Zr had a slightly lower hydrocarbon production rate than 90Fe10Zr). Berry et al. [26] proposed that Zr^{4+} can interact with O atoms of CO, thus weakening the C–O bond and thereby increasing carbide formation. In contrast, O'Brien et al. [10] reported that the adding Zr to an ultrafine Fe catalyst did not improve the catalyst activity. These divergent findings may be related to differences in catalyst composition and/or preparation in the two studies.

Table 3
Catalyst activities and selectivities for the Fe-based catalysts

Catalyst[a]	Maximum rate[b] (μmol of C/(g s))		SS rate[b] (μmol of C/(g s))		Maximum TOF_{chem}[c] (s^{-1}) × 10^2	%Hydrocarbon selectivity at SS[b,d]					%Olefin[b] (C_2–C_4 fraction)	α[b] (C_3–C_6)
	CO_2	Total HC	CO_2	Total HC		C_1	C_2	C_3	C_4	C_5–C_8		
100Fe	0.50	0.78	0.13	0.43	0.53	27	29	23	16	5	74	0.35
97Fe3Cr	0.96	1.34	0.23	0.50	0.62	29	28	25	13	6	74	0.35
95Fe5Cr	1.14	1.59	0.25	0.52	0.59	29	26	25	13	8	75	0.36
93Fe7Cr	1.18	1.56	0.24	0.50	0.69	28	26	25	13	8	75	0.37
90Fe10Cr	0.87	1.26	0.16	0.36	0.66	26	28	31	12	4	77	0.36
95Fe5Mn	0.99	1.58	0.24	0.72	0.83	29	26	22	18	6	82	0.35
93Fe7Mn	1.10	1.64	0.28	0.73	0.88	29	25	21	18	6	83	0.33
90Fe10Mn	1.24	1.73	0.30	0.76	0.97	32	26	22	18	2	81	0.35
80Fe20Mn	1.28	1.78	0.35	0.80	1.09	34	26	22	16	2	83	0.33
97Fe3Zr	1.01	1.35	0.20	0.53	0.79	27	26	21	19	6	78	0.34
95Fe5Zr	1.27	1.77	0.24	0.57	0.90	28	26	23	21	2	81	0.32
90Fe10Zr	1.75	2.24	0.32	0.58	1.04	31	27	24	12	6	82	0.34
86Fe14Zr	2.07	2.05	0.28	0.55	0.94	29	25	21	19	5	85	0.35

[a] All catalysts also contained 5Cu and 17Si.
[b] Max error = ±3%. At steady-state (5 h TOS).
[c] Calculated from TOF_{chem} = reaction rate (at the maximum activity)/[2 × (total CO chemisorbed)]. Max error = ±10%.
[d] Based on atomic carbon.

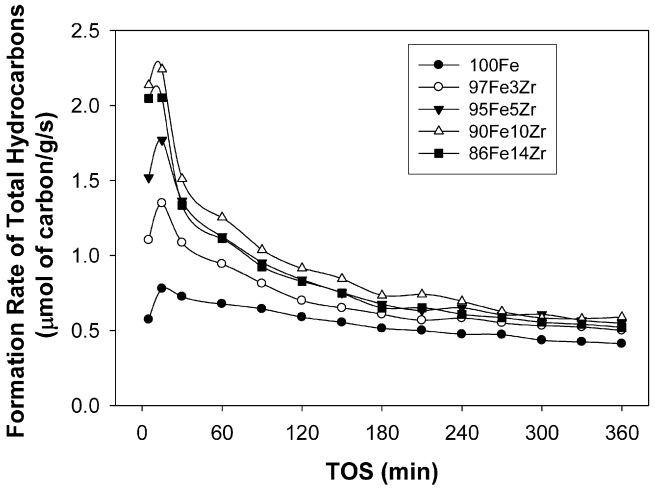

Fig. 6. Formation rates of (a) total hydrocarbons (C_1–C_8) and (b) CO_2 for the Zr-promoted catalysts.

Table 3 summarizes reaction rates, TOF_{chem}s (based on CO chemisorption), %hydrocarbon selectivities on a carbon basis, %C_2–C_4 olefin (ethylene, propylene, and butene) selectivities, and chain growth probabilities (α) of the various Fe-based catalysts. The TOF_{chem} for the FeMe catalysts generally increased with increasing concentration. The %selectivity to hydrocarbons and α (ca. 0.32–0.37) were similar for all catalysts, regardless of amount or type of added Me, within the limits of experimental error. The selectivity for C_2–C_4 olefins was improved slightly by the addition of Mn or Zr.

Fig. 7 replots the activities of FeMe at the optimum concentration of added metal (95Fe5Cr, 80Fe20Mn, and 90Fe10Zr) for comparison purposes. 90Fe10Zr initially exhibited the highest activities for CO hydrogenation and the WGS reaction but rapidly deactivated and became less active at long TOS. 80Fe20Mn was the most active and stable catalyst overall. Jensen and Massoth [27] have suggested that the promoting effect of Mn on the activity of Fe catalysts may be due to the ability of Mn oxide to modify the electronic state of Fe by being an electron donor, like alkali metals. However, Herranz et al. [28] proposed that active carbonaceous intermediate species are stabilized by the presence of Mn.

3.2.2. Steady-state isotopic transient kinetic analysis

We carried out an in-depth investigation using SSITKA to evaluate the affect of adding Cr, Mn, and Zr on the surface reaction kinetic parameters. In particular, we explored whether the average surface residence time for reaction (τ, inversely related to the site TOF), the number of active surface reaction intermediates (N), or both were modified by the presence of these three metals. Due to the fragmentation and overlapping among isotopically labeled hydrocarbon molecules (especially higher hydrocarbons), which hinders direct isotopic analysis by mass spectrometry (MS), we carried out SSITKA under methanation conditions with a H_2:CO ratio of 20:1 to obtain CH_4 as the primary product. This is adequate for the present study because the primary effect of the third metal is on activity, not selectivity. The system setup and methods used to calculate the surface residence time (τ_{CH_4}) and concentration of active surface intermediates (N_{CH_4}) are described in detail elsewhere [13,14].

Fig. 8 shows the formation rates of CH_4 for 100Fe, 95Fe5Cr, 80Fe20Mn, and 90Fe10Zr, with Cr, Mn, and Zr added at the optimum concentrations. As expected, greater catalytic activity with less deactivation was observed under a higher partial pressure of H_2 [29]. A positive affect of adding Cr, Mn, and Zr on the activity of the Fe catalyst also was observed. At 6 h TOS, the formation rate of CH_4 for the FeMe catalysts was at least double that for the base 100Fe catalyst; however, the degree of increased activity seen for 80Fe20Mn was less than that of 95Fe5Cr and 90Fe10Zr, whereas the selectivity for CH_4 was similar in the four Fe catalysts, at about 53–61% (not shown). This result does not contradict the

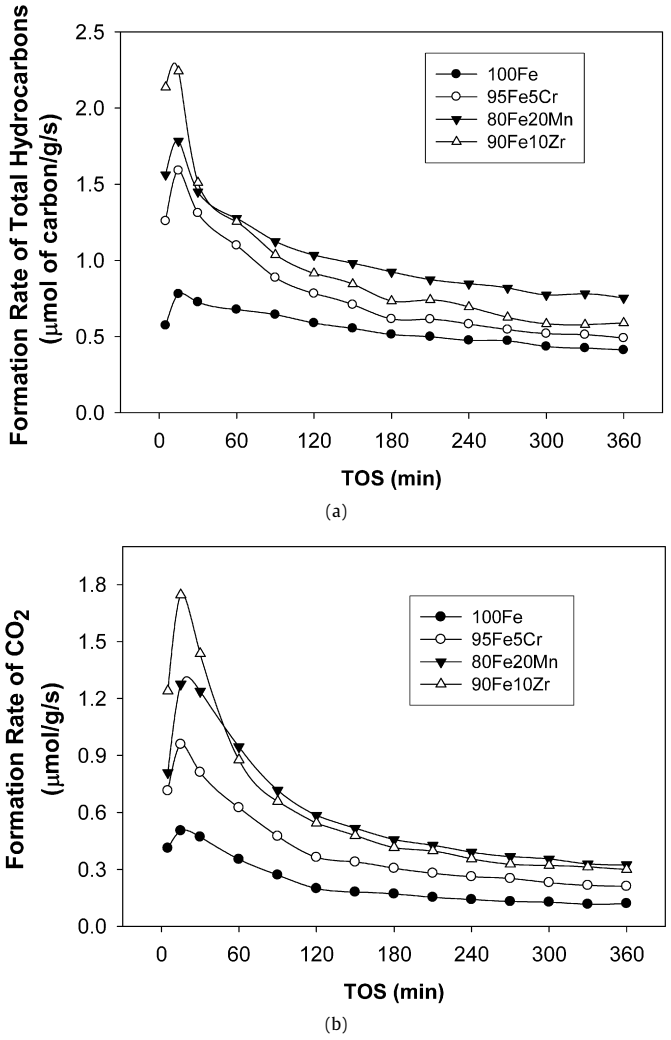

Fig. 7. Catalyst activities for (a) CO hydrogenation and (b) WGS at the optimum concentrations of added Cr, Mn, and Zr.

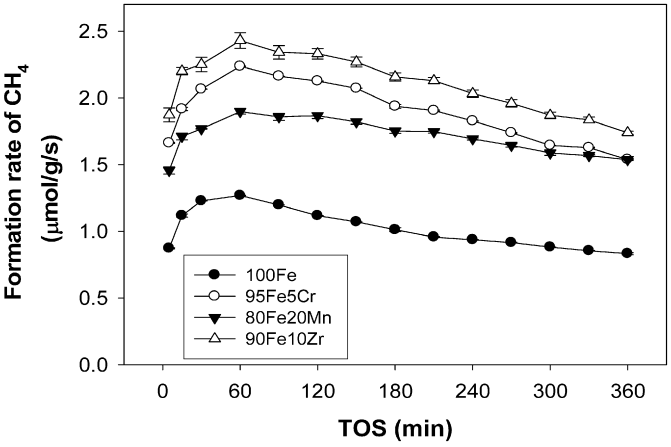

Fig. 8. Formation rates of CH_4 during SSITKA on the various Fe-based catalysts (with Cr, Mn and Zr at the optimum concentrations).

findings observed when the reaction was carried out at a H_2:CO ratio of 2:1, where the activity of 80Fe20Mn was higher than that of 95Fe5Cr and 90Fe10Zr. As Fig. 8 shows, the reaction rate was more stable on 80Fe20Mn and decreased more rapidly with TOS for 95Fe5Cr and 90Fe10Zr. Therefore (although it takes longer at a H_2/CO ratio of 20 than at a ratio of 2), eventually the activities of the 95Fe5Cr and 90Fe10Zr catalysts will drop below that of the more stable Fe20Mn catalyst.

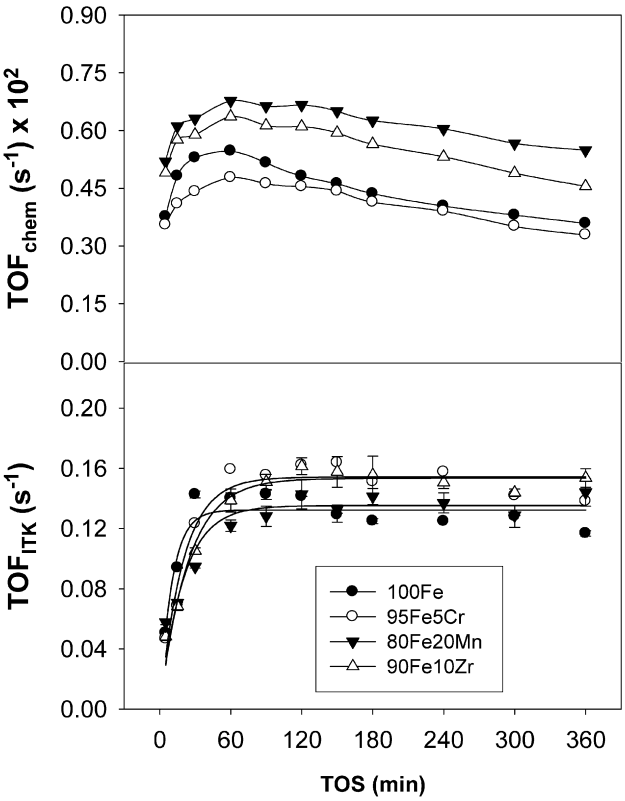

Fig. 9. Comparisons of TOF_{ITK} (from SSITKA) with TOF_{chem} for the various Fe-based catalysts (with Cr, Mn and Zr at the optimum concentrations).

We determined the average surface residence times of CO (τ_{CO}) and CH_4 (τ_{CH_4}) using SSITKA. The concentrations of active surface intermediates of CO (N_{CO}) and of CH_4 (N_{CH_4}) were calculated by $N_{CO} = \tau_{CO} \times (\text{flowrate}_{CO})$ and $N_{CH_4} = \tau_{CH_4} \times (\text{rate}_{CH_4})$, respectively [14]. The interpretation of τ_{CO} is not straightforward, however, because although τ_{CO} is an average surface residence time over every CO molecule, not all CO molecules adsorb on the catalyst in a differential reactor with a high flow rate. In contrast, the interpretation of τ_{CH_4} is more meaningful, because every CH_4 was formed on the catalyst. The intrinsic site activity leading to CH_4 can be estimated from $1/\tau_{CH_4} = \text{rate}_{CH_4}/N_{CH_4} = TOF_{ITK}$.

We compared TOF_{chem} (CH_4 formation) results calculated based on CO chemisorption at 35 °C with TOF_{ITK} (CH_4 formation) determined using SSITKA. The results, shown in Fig. 9, demonstrate similar TOF_{chem} values for 80Fe20Mn and 90Fe10Zr, higher than those for 95Fe5Cr and 100Fe. In contrast, the TOF_{ITK} values were essentially similar for all of the Fe catalysts, within the limits of experimental error. Because TOF_{ITK} is more meaningful in terms of the reaction on the active sites, this finding implies that the average site activity of the Fe catalyst was not significantly altered by the presence of any third-metal promoter, suggesting that the active sites also may have been identical on all of the Fe catalysts. Fig. 9 also shows that the average site activity estimated using CO chemisorption (TOF_{chem}) was approximately an order of magnitude lower than that determined using SSITKA (TOF_{ITK}), due to overestimation of the number of active reaction sites by CO chemisorption. This observation is in agreement with previous findings of our research group [13,30].

Fig. 10 compares the number of active surface intermediates leading to CH_4 (N_{CH_4}) with TOS for the Fe catalysts with and without added Cr, Mn, or Zr at the optimum concentrations. N_{CH_4}

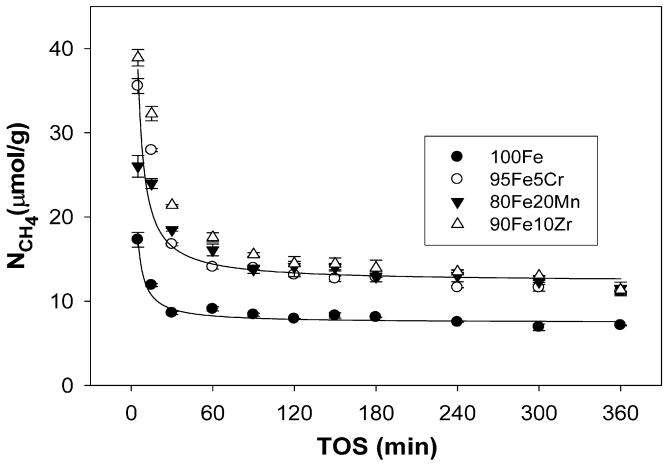

Fig. 10. The concentration of active surface intermediates of CH_4 (N_{CH_4}) vs TOS on the various Fe-based catalysts (with Cr, Mn and Zr at the optimum concentrations) (error bars are given to emphasize the reproducibility of the results).

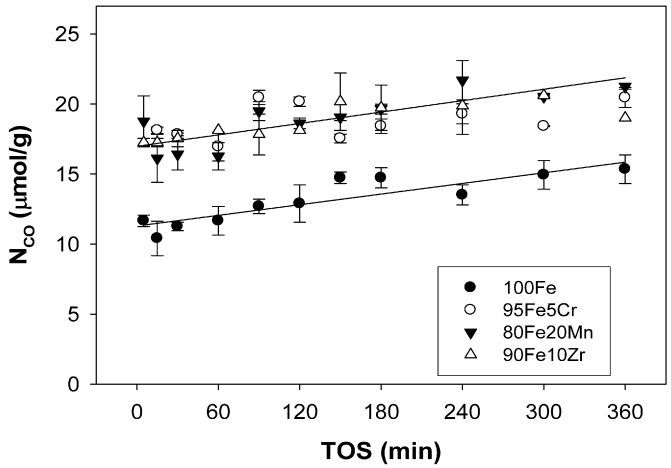

Fig. 11. The concentration of active surface intermediates of CO (N_{CO}) vs TOS on the various Fe-based catalysts (with Cr, Mn and Zr at the optimum concentrations) (error bars are given to emphasize the reproducibility of the results).

for the third-metal-promoted Fe catalysts (i.e., 95Fe5Cr, 80Fe20Mn, and 90Fe10Zr) was double that for 100Fe. These findings, in conjunction with the results for site activity ($1/\tau_{CH_4} = TOF_{ITK}$, Fig. 9), lead us to conclude that the enhanced activity of the Fe catalyst with third-metal promotion was due primarily to an increase in the number of active surface intermediates and thus the number of active sites. The positive affect of third-metal promotion on the concentration of active surface intermediates possibly could be related to the greater number of surface-exposed Fe^0 atoms in the FeMe catalysts.

Fig. 10 also shows that N_{CH_4} dropped significantly with TOS before achieving a steady-state value after ca. 1 h of reaction. The decrease in N_{CH_4} for 80Fe20Mn was not as significant as that for 100Fe, 95Fe5Cr, and 90Fe10Zr, although its steady-state value was similar to those of the initially more active 95Fe5Cr and 90Fe10Zr. This finding also demonstrates the greater stability of the 80Fe20Mn catalyst. The decline in N_{CH_4} could have been due to site blockage by initial carbon deposition. It was found that significant amounts of carbon deposited on the surface of the 80Fe20Mn catalyst during the initial 60 min TOS [64% of the amount of carbon deposited during 6 h of reaction (3.11 mmol/g)]; however, the surface concentration of reversibly adsorbed CO (N_{CO}) under reaction conditions actually increased slightly with TOS for all of the Fe catalysts and did not appear to be affected by carbon deposition. The Fe catalysts with third-metal promotion exhibited higher N_{CO} values than 100Fe (Fig. 11).

Comparing changes in catalyst rate of methanation and TOF_{ITK} (Figs. 8 and 9) shows that the induction period of reaction likely resulted from an increase in the average site activity of the catalyst. Some have speculated that this increase is related to the formation of Fe carbides, which have been proposed to be the active Fe phase for FTS [25,31–33]. The duration of the induction period may depend on the CO concentration. Comparing the reaction rate profile of Fe catalysts at different H_2:CO ratios shows that a longer induction period was required (from 15 min to 60 min TOS) as P_{CO} decreased (from 0.15 to 0.045 atm, i.e., a H_2:CO ratio of 2:1 vs 20:1).

4. Conclusion

In this work, we have shown that the addition of Cr, Mn, and Zr increased the activity of a precipitated $FeCuSiO_2$ catalyst for both CO hydrogenation and the WGS reaction and also promoted the dispersion of Fe, but had no affect on BET surface area, %Fe reducibility, %hydrocarbon selectivity, or chain growth probability (α). The reaction site activities of the catalysts ($1/\tau_{CH_4} = TOF_{ITK}$) were similar regardless of type of third metal added, indicating that promoting Fe catalysts with Cr, Mn or Zr had no affect on the intrinsic site activity of the base catalyst and suggesting that the active sites were similar. The high activity observed for the Cr-, Mn-, and Zr-promoted Fe catalysts appears to be linked to a greater number of active surface intermediates leading to product and, by inference, a greater number of active sites.

Acknowledgments

This paper is based on work supported by the National Association of State Energy Offices (NASEO) through grant DE-FC36-03G013026. Any opinions, findings, and conclusions or recommendations expressed herein are those of the authors and do not necessarily reflect the views of the NASEO.

References

[1] http://www.energy.gov. as of January 15th, 2008.
[2] R.B. Anderson, The Fischer–Tropsch Synthesis, Academic Press, Orlando, FL, 1984.
[3] H.H. Storch, N. Golumbic, R.B. Anderson, The Fischer–Tropsch and Related Synthesis, Wiley, New York, 1951.
[4] T.C. Bromfield, R. Visagie, Chromium oxide incorporation into precipitated iron-based Fischer–Tropsch catalysts for increased production of oxygenates and branched hydrocarbons, Patent # WO2005/049765A1 (2005) USA.
[5] C. Wang, Q.X. Wang, X.D. Sun, L.Y. Xu, Catal. Lett. 105 (2005) 93–101.
[6] L. Bai, H.W. Xiang, Y.W. Li, Y.Z. Han, B. Zhong, Fuel 81 (2002) 1577–1581.
[7] R. Malessa, M. Baerns, Ind. Eng. Chem. Res. 27 (1988) 279–283.
[8] N. Lohitharn, J.G. Goodwin Jr., E. Lotero, J. Catal. 255 (2008) 104–113.
[9] Y. Yang, H.W. Xiang, Y.Y. Xu, L. Bai, Y.W. Li, Appl. Catal. A Gen. 266 (2004) 181–194.
[10] R.J. Obrien, L.G. Xu, D.R. Milburn, Y.X. Li, K.J. Klabunde, B.H. Davis, Top. Catal. 2 (1995) 1–15.
[11] D.B. Bukur, X.S. Lang, J.A. Rossin, W.H. Zimmerman, M.P. Rosynek, E.B. Yeh, C.P. Li, Ind. Eng. Chem. Res. 28 (1989) 1130–1140.
[12] H.J. Jung, M.A. Vannice, L.N. Mulay, R.M. Stanfield, W.N. Delgass, J. Catal. 76 (1982) 208–224.
[13] J.G. Goodwin Jr., S.Y. Kim, W.D. Rhodes, in: J.J. Spivey, G.W. Roberts (Eds.), Catalysis, The Royal Society of Chemistry, chap. 8.
[14] S. Hammache, J.G. Goodwin, S.L. Shannon, S.Y. Kim, Encyclopedia Surface Colloid Sci. 1 (2002) 2445–2454.
[15] M.E. Dry, The Fischer–Tropsch Synthesis, Springer-Verlag, New York, 1981, pp. 159–255.
[16] K. Sudsakorn, J.G. Goodwin, K. Jothimurugesan, A.A. Adeyiga, Ind. Eng. Chem. Res. 40 (2001) 4778–4784.
[17] D.B. Bukur, M. Koranne, X.S. Lang, K.R.P.M. Roa, G.P. Huffman, Appl. Catal. A Gen. 126 (1995) 85–113.
[18] S.Z. Li, S. Krishnamoorthy, A.W. Li, G.D. Meitzner, E. Iglesia, J. Catal. 206 (2002) 202–217.

[19] D.B. Bukur, C. Sivaraj, Appl. Catal. A Gen. 231 (2002) 201–214.
[20] K. Jothimurugesan, J.G. Goodwin, S.K. Gangwal, J.J. Spivey, Catal. Today 58 (2000) 335–344.
[21] X. Ge, H. Zou, J. Wang, J.Y. Shen, React. Kinet. Catal. Lett. 85 (2005) 253–260.
[22] Z.C. Tao, Y. Yang, H.J. Wan, T.Z. Li, X. An, H.W. Xiang, Y.W. Li, Catal. Lett. 114 (2007) 161–168.
[23] K.B. Jensen, F.E. Massoth, J. Catal. 92 (1985) 98–108.
[24] M.D. Lee, J.F. Lee, C.S. Chang, T.Y. Dong, Appl. Catal. 72 (1991) 267–281.
[25] J.W. Niemantsverdriet, A.M. van der Kraan, W.L. van Dijk, H.S. van der Baan, J. Phys. Chem. 84 (1980) 3363–3370.
[26] F.J. Berry, S. Jobsen, M.R. Smith, Hyperfine Interact. 46 (1989) 607–611.
[27] K.B. Jensen, F.E. Massoth, J. Catal. 92 (1985) 109–118.
[28] T. Herranz, S. Rojas, F.J. Perez-Alonso, M. Ojeda, P. Terreros, J.L.G. Fierro, J. Catal. 243 (2006) 199–211.
[29] G.P. Van der Laan, A.A.C.M. Beenackers, Catal. Rev. 41 (1999) 255–318.
[30] K. Sudsakorn, J.G. Goodwin, A.A. Adeyiga, J. Catal. 213 (2003) 204–210.
[31] S.Z. Li, R.J. O'Brien, G.D. Meitzner, H. Hamdeh, B.H. Davis, E. Iglesia, Appl. Catal. A Gen. 219 (2001) 215–222.
[32] G. Lecaer, J.M. Dubois, M. Pijolat, V. Perrichon, P. Bussiere, J. Phys. Chem. 86 (1982) 4799–4808.
[33] W.S. Ning, N. Koizumi, H. Chang, T. Mochizuki, T. Itoh, M. Yamada, Appl. Catal. A Gen. 312 (2006) 35–44.